# Chebyshev polynomial approach to Loschmidt echo: Application to quench dynamics in two-dimensional quasicrystals

Niaz Ali Khan, Shihao Ye, Ziheng Zhou, Shujie Cheng, and Gao Xianlong*
*Department of Physics, Zhejiang Normal University, Jinhua 321004, People's Republic of China*

(Received 20 December 2023; accepted 6 June 2024; published 25 June 2024)

The understanding of quantum phase transitions in disordered or quasicrystal media is a central issue in condensed matter physics. In this paper we investigate localization properties of the two-dimensional Aubry-André model. We find that the system exhibits self-duality for the transformation between position and momentum spaces at a critical quasiperiodic potential, leading to an energy-independent Anderson transition. Most importantly, we present the implementation of an efficient and accurate algorithm based on the Chebyshev polynomial expansion of the Loschmidt echo, which characterizes the nonequilibrium dynamics of quantum quenched quasiperiodic systems. We analytically prove that the system under quench dynamics displays dynamical quantum phase transitions and further provide numerical verification by computing the polynomial expansion of the Loschmidt echo. Our results may provide insight into the realization of electronic transport in experiments.

DOI: 10.1103/PhysRevE.109.065311

## I. INTRODUCTION

The Aubry-André model [1] has been extensively studied in the context of electronic transport and topology in condensed matter physics. Most essentially, the periodicity of the diagonal potential is incommensurate with the lattice periodicity, which turns out to be the most peculiar property of the model [2–7]. Moreover, the energy spectrum of the model is symmetric ($E \leftrightarrow -E$) with respect to zero energy in the noninteracting nearest-neighbor restrictions, but loses the symmetry properties in the presence of non-Hermiticity [8–10], next nearest-neighbor hopping [11], and generalized Aubry-André quasiperiodic site energies [12,13]. Furthermore, the model exhibits a self-duality extended to the localization transition at a critical point [14]. The Aubry-André model has been experimentally realized in ultracold atoms [15,16], photonic crystals [17], and polariton condensates [18]. Recently, a quantum critical phase transition has been realized experimentally in the generalized Aubry-André model with superconducting circuits [19].

A mobility edge [4,5,20–22] demarcates the localized and delocalized regimes, opening up a new avenue for a better understanding of electronic properties in disordered systems. It is well established that the standard one-dimensional (1D) Aubry-André model [1] is self-dual under the Fourier transformation at the critical quasiperiodic potential, leading to a quantum phase transition without mobility edges. However, the generalized [5,21] and non-Hermitian [8,9,23–26] 1D Aubry-André model possesses a self-duality relation with mobility edges separating extended and localized states for a fixed incommensurate potential strength. Moreover, a self-duality with an exact mobility edge has been encountered in the two-dimensional (2D) non-Hermitian quasicrystal model [27] with parity-time $\mathcal{PT}$ symmetry. Remarkably, the system with a mobility edge exhibits large thermoelectric effects, which are highly applicable in thermoelectric devices [28].

Quantum phase transition in a nonequilibrium setting under a quenching process is one of the most active areas of research in condensed matter physics [29–45]. Quantum quenches refer to an abrupt change of the system parameters that govern time evolution and can lead to dynamical quantum phase transitions (DQPTs), characterized by the nonanalytic nature of the Loschmidt echo [32]. A Loschmidt echo is a measure of the return probability of the ground state during the time evolution of the initial state [32–34], particularly important in the characterization of the nonequilibrium phase transition [37]. The quench process comes in a variety of systems, including atomic Mott insulators [46], Aubry-André models [27,32,41,42], the Lipkin-Meshkov-Glick model [34], Aubry-André models with a $p$-wave superconducting pairing [35], standard Anderson models [33], 2D $p$-wave topological superconductors [40], 2D transverse-field Ising models [47], and correlated Anderson models [42]. Recently, DQPTs have been experimentally performed under the quench dynamics of out-of-time-ordered correlators on a nuclear magnetic resonance simulator [48].

Quantum simulations of lattice models are one of the significant challenges in understanding localization properties in large-scale condensed matter systems [49–52]. The main task in this simulation is the eigendecomposition of a Hamiltonian matrix, which requires $O(N^3)$ numerical complexity for an $N$-dimensional dense Hamiltonian matrix [49]. The understanding of the electronic transport of quantum materials has been significantly enriched by the implementation of the kernel polynomial method (KPM) [50–59]. The KPM is a polynomial expansion-based algorithm and can efficiently compute various physical quantities without diagonalizing the Hamiltonian matrix. It has been successfully applied in

*Contact author: gaoxl@zjnu.edu.cn

 

calculating the Green's functions of a superconductor [60], the single-particle spectral function [56], the Thouless expression of localization length [61], the conductance of twisted bilayer graphene [62], topological spin excitations in non-Hermitian spin chains [58], and dynamical correlations at zero temperature [53,54]. The numerical calculations of Loschmidt echo are computationally expensive for methods like exact diagonalization, which are limited to small system sizes. Remarkably, the KPM technique has been tremendously applied for the simulations of Loschmidt echo in large-scale 1D systems [63].

The Aubry-André model has been the subject of extensive research in the context of quantum transport. Most of the up-to-date research is devoted to 1D systems [29–43], and the results for 2D and three-dimensional systems are rare, although from an experimental point of view, these dimensions are the most interesting [47]. In this paper, we uncover the electronic properties of a noninteracting 2D Aubry-André model in the context of tight binding with an incommensurate on-site potential. The system exhibits self-duality and exhibits an insulator-metal transition at the critical strength of the quasiperiodic potential without a mobility edge. Furthermore, we investigate the nonequilibrium dynamics of the model via a swift change in the strength of the quasiperiodic potential. Taking advantage of the highly efficient polynomial expansion-based method, which enables the accurate calculations of the Loschmidt echo to be possible, we explore large-scale numerical simulations of the quench dynamics of the model. It turns out that the quench dynamics under certain conditions reveal the nonanalyticities of the Loschmidt echo at critical times, reflecting the DQPTs in the system. Moreover, we numerically explore that the finite system under quench dynamics displays DQPTs when an initial reference extended (localized) state is quenched into a localized (extended) time-evolved state.

The structure of our paper is as follows: Sec. II discusses a tight-binding 2D Aubry-André model with nearest-neighbor interactions. Furthermore, we analyze the self-duality relations without mobility edges in the model analytically, which is verified by the numerical calculations in the framework of IPR and NPR. Section III briefly reviews the quench dynamics formalism based on the Loschmidt echo and focuses on the numerical calculations based on the polynomial expansion method. Section IV demonstrates the numerical complexity of the polynomial expansions of the Loschmidt echo. The last section summarizes our conclusions.

## II. THE AUBRY-ANDRÉ MODEL

This section is devoted to a comprehensive study of the 2D Aubry-André model and discusses the dynamics properties of the system in an equilibrium setting. The model consists of noninteracting spinless fermions on a square lattice with nearest-neighbor interactions and periodic boundary conditions (PBC). The Hamiltonian of the system has the general form [64–66]

$$\hat{H} = -t\sum_{x,y}\left(c^{\dagger}_{x,y}c_{x+1,y} + c^{\dagger}_{x,y}c_{x,y+1} + \text{H.c.}\right) - \sum_{x,y}\varepsilon_{x,y}n_{x,y}, \tag{1}$$

where $n_{x,y} = c^{\dagger}_{x,y}c_{x,y}$ denotes the number operator and $c^{\dagger}_{x,y}(c_{x,y})$ is a free fermionic creation (annihilation) operator at site $(x, y)$, where $x$ and $y$ are the 2D spatial coordinates of the lattice. The parameter $\varepsilon_{x,y}$ denotes the incommensurate energy of an electron at the $(x, y)$-th site of the lattice of size $N = L \times L$ and $t$ is the hopping integral (transfer energy) between the nearest-neighboring sites. It is important to note that all energy scales are measured in units of $t$, where $t$ is set to unity. For this model, the lattice site energy is the quasiperiodic potential given by [64]

$$\varepsilon_{x,y} = \lambda[\cos(2\pi\gamma x) + \cos(2\pi\gamma y)], \tag{2}$$

where $\lambda$ denotes the modulation amplitude of the incommensurate diagonal energy, with $\gamma = (\sqrt{5}-1)/2$ being an irrational number. The quasiperiodic potential will restrict electrons to a finite region of space under certain conditions.

The Hamiltonian of the system can also be expressed in the form of the eigenvalues equation:

$$t\left(\Psi_{x+1,y} + \Psi_{x-1,y} + \Psi_{x,y+1} + \Psi_{x,y-1}\right) = (E - \varepsilon_{x,y})\Psi_{x,y}, \tag{3}$$

where $\Psi_{x,y}$ is the wave function at site $(x, y)$ of the 2D Aubry-André model. To examine the self-duality in the system, we introduce a duality Fourier transformation:

$$\Phi_{p,q} = \frac{1}{\sqrt{N}}\sum_{xy}\Psi_{x,y}\exp\left[i(2\pi\gamma xp + 2\pi\gamma yq)\right]. \tag{4}$$

Substituting $\Phi_{p,q}$ in (3) gives

$$\frac{\lambda}{2}\left(\Phi_{p+1,q} + \Phi_{p-1,q} + \Phi_{p,q+1} + \Phi_{p,q-1}\right) = (E - \varepsilon_{p,q})\Phi_{p,q}, \tag{5}$$

where $\varepsilon_{p,q} = 2t[\cos(2\pi\gamma p) + \cos(2\pi\gamma q)]$. The expression (4) transforms the real-space Hamiltonian into momentum space. Most importantly, the 2D quasicrystal is self-dual under the position-momentum transformation by interchanging $\lambda = 2t$, leading to an energy-independent metal-insulator transition in the system.

To explicitly verify the phenomenon of the metal-insulator transition, we numerically calculate the inverse participation ratio (IPR) and normalized participation ratio (NPR), which are the most reliable theoretical tools to characterize the Anderson transition. The IPR for a single-particle system is defined as

$$\text{IPR} = \frac{\sum_{x,y}|\psi_{x,y}|^4}{\left(\sum_{x,y}|\psi_{x,y}|^2\right)^2}, \tag{6}$$

where $\psi_{x,y}$ is the normalized eigenstate of the system's Hamiltonian, i.e., $\sum_{x,y}|\psi_{x,y}|^2 = 1$. In general, the IPR for an extended state is proportional to $1/\sqrt{N}$, which approaches zero in the thermodynamic limit. On the other hand, the IPR tends toward unity in a strongly localized state of the system. On the other hand, the NPR is defined as

$$\text{NPR} = \frac{1}{N\sum_{x,y}|\psi_{x,y}|^4}. \tag{7}$$

The NPR is a complementary quantity of the IPR, typically approaches unity for an extended state, and goes to zero for a localized state of the system in the thermodynamic limit.

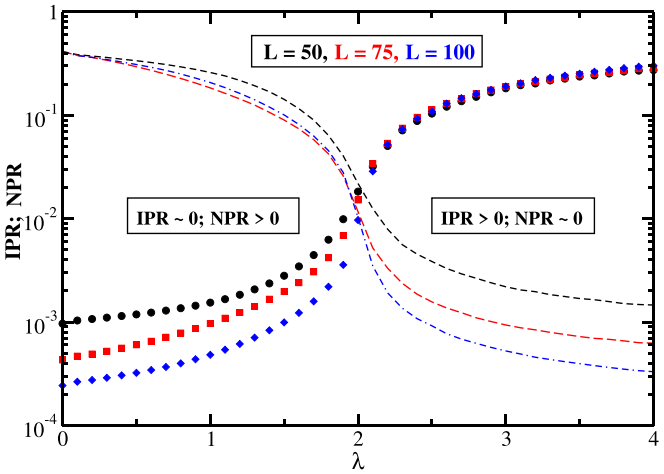


FIG. 1. IPR (symbols) and NPR (dashed curves) of the 2D Aubry-André model with various linear system sizes in log-linear scale.

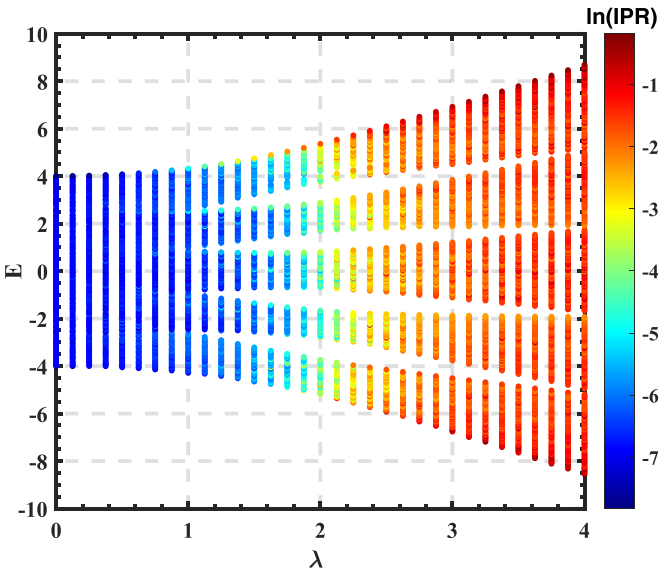


FIG. 2. Phase diagrams of the 2D Aubry-André model in the energy-potential plane. The phase diagram is obtained by computing the logarithm of the IPR of the system with linear size $L = 100$ and averaged over all eigenstates.

In Fig. 1 we present the IPR and NPR averaged over all eigenstates of the 2D quasicrystal with different linear system sizes. The IPR (NPR) shows strong system-size dependence in the weak (strong) potential regime, indicating the extended nature of the system. At stronger potential strength, the IPR is nearly size-independent and approaches unity, reflecting the localized nature of the system. On the other hand, the NPR turns out size-independent and tends to unity in the vanishing potential strength in the thermodynamic limit. However, a small deviation of the NPR is observed for $L = 50$ in the weak potential limit due to a small system size effect. One can see clearly that for $\lambda \lesssim 2$ the IPR approaches zero, whereas the NPR is finite, resulting in delocalized eigenstates of the system. On the contrary, the IPR is finite and the NPR approaches zero for $\lambda \gtrsim 2$, reflecting the insulating behavior of the system. At a critical point, the IPR starts to increase while the NPR drops to zero. Figure 2 demonstrates the logarithm of the IPR of different eigenstates as a function of the corresponding eigenvalues $E$ and incommensurate potential strength under PBC. It is pointed out that the metal-insulator transition happens at $\lambda = 2t$ with no mobility edge emerging in the spectrum.

The fidelity susceptibility is a diagnostic tool of the quantum phase transition extensively studied in various physical systems [67–77]. In general, the system Hamiltonian (1) can be expressed as

$$\hat{H} = \hat{H}_0 + \lambda \hat{H}_1, \tag{8}$$

where $\hat{H}_0$ is the kinetic, $\hat{H}_1$ is the on-site potential part of the Hamiltonian, and $\lambda$ is a potential controlling parameter, triggering a quantum phase transition at critical strength. The ground-state fidelity, $F(\lambda, \delta\lambda)$, is the overlap between the ground states $|\Psi_0(\lambda)\rangle$ and $|\Psi_0(\lambda + \delta\lambda)\rangle$:

$$F(\lambda, \delta\lambda) = |\langle \Psi_0(\lambda) | \Psi_0(\lambda + \delta\lambda)\rangle|. \tag{9}$$

It is important to mention that the states $|\Psi_0(\lambda)\rangle$ and $|\Psi_0(\lambda + \delta\lambda)\rangle$ are the initial ground states of the system's Hamiltonian at potential $\lambda$ and $\lambda + \delta\lambda$, respectively. The fidelity of the system depends on the strength of $\lambda$ and $\delta\lambda$, where $\lambda \gg \delta\lambda$. The fidelity turns out to be unity when two ground states are in the same phase: $\Psi_0(\lambda) = \Psi_0(\lambda + \delta\lambda)$. On the other hand, fidelity exhibits a sharp dip at the critical point, where the two ground states are qualitatively in different phases. In general, the $F(\lambda, \delta\lambda)$ vanishes exponentially with the system size at the quantum critical point; therefore, the concept of fidelity susceptibility [67,68], $X_F(\lambda)$, naturally appears to be the dominant contribution to the fidelity in the limit $\delta\lambda \to 0$, defined as

$$X_F(\lambda) = -2 \lim_{\delta\lambda \to 0} \frac{\ln F(\lambda, \delta\lambda)}{(\delta\lambda)^2}. \tag{10}$$

Figure 3 shows the rescaled fidelity susceptibility of the model as a function of incommensurate potential strength $\lambda$ with different linear system sizes in the log-linear scale. The $X_F(\lambda)\delta\lambda^2$ exhibits a peak near the critical point and becomes more profound with increasing sizes. In fact, the peak value of the $X_F(\lambda)\delta\lambda^2$ increases exponentially with the system's size, as shown by the magenta dashed line in the inset. The divergence behavior of the fidelity susceptibility at $\lambda = 2$ signals the metal-insulator transition of the system.

## III. NONEQUILIBRIUM QUENCH DYNAMICS

A quantum quench process is the simplest paradigmatic protocol for studying nonequilibrium dynamics, where a swift change of the system parameters can independently control the time evolution of the system [29,31,78]. The fundamental object that describes the dynamical properties of systems is the Loschmidt echo [29,32], which is a measure of the overlap between an initial ground and its time-evolved state. Let $\alpha$ be the prequench system parameter that controls the strength of the on-site potential of the system Hamiltonian $H(\alpha)$. Applying the eigenproblem, one can get the normalized ground state $|\Psi(\alpha)\rangle$ of the system at time $\tau = 0$. However, after the quenching process, the Hamiltonian $H(\beta)$ governs the time

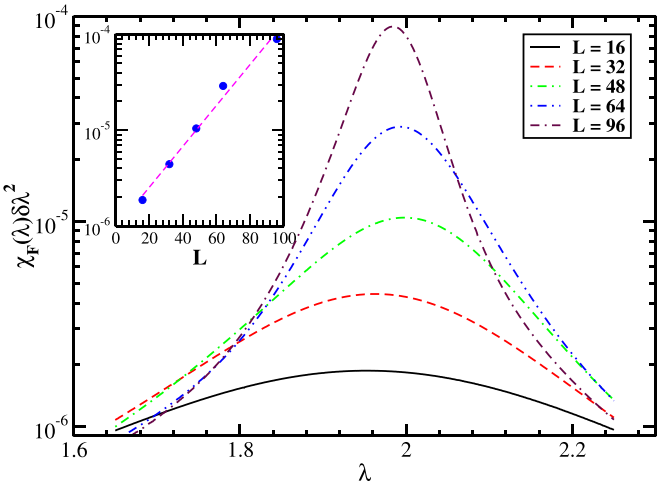


FIG. 3. The rescaled fidelity susceptibility of the 2D Aubry-André model as a function of $\lambda$ at $\delta\lambda = 10^{-3}$ for different linear system sizes in log-linear scale. The $X(\lambda)\delta\lambda^2$ has a peak near the critical potential strength that increases exponentially with increasing size. Inset: Maximum of $X_F(\lambda)\delta\lambda^2$ as a function linear system size. The $X_F(\lambda)\delta\lambda^2$ are very well fitted by a curve $y \approx e^{0.5x}$ (magenta dashed line).

evolution of the system at certain times $\tau > 0$, reaching the unitary evolving state [27,32,42],

$$|\Psi(\alpha, \beta, \tau)\rangle = e^{-i\tau H(\beta)}|\Psi(\alpha)\rangle, \tag{11}$$

where $\beta$ controls the strength of the postquench diagonal potential. In particular, the quenching process changes the ground state $|\Psi(\alpha)\rangle$ under the postquench Hamiltonian $H(\beta)$ and starts to experience the time evolution for $\tau > 0$. A Loschmidt amplitude, $G(\alpha, \beta, \tau)$, can be applied to characterize the overlap between the initial ground and time-evolved state,

$$G(\alpha, \beta, \tau) = \langle\Psi(\alpha)|\Psi(\alpha, \beta, \tau)\rangle. \tag{12}$$

A Loschmidt echo, $L(\alpha, \beta, \tau)$, is the squared modulus of the Loschmidt amplitude, analogous to the dynamical version of the ground-state fidelity (return probability), and has the form [27,32]

$$L(\alpha, \beta, \tau) \equiv |G(\alpha, \beta, \tau)|^2 = |\langle\Psi(\alpha)|\Psi(\alpha, \beta, \tau)\rangle|^2. \tag{13}$$

It is well known that the Loschmidt echo typically decays from unity, oscillating with constant frequency and damping amplitude to zero after some time interval [32]. However, this strongly depends on the prequench and postquench system Hamiltonians [42]. More importantly, the echo periodically approaches zero at critical times under certain conditions, characterizing the DQPTs.

It is worthwhile to mention that the Loschmidt echo plays a fundamental role in characterizing the quench dynamics of the system. The singular behavior of the logarithm of the Loschmidt echo, termed the dynamical quantum phase transition, has been the subject of several experimental and theoretical investigations. In order to get a better understanding, we analytically calculate the Loschmidt echo of the quench processes between states with prequench on-site potential $\lambda_i = 0(\infty)$ and postquench modulation potential $\lambda_f = \infty(0)$ in the thermodynamic limit. In the first case, the initial eigenstates of the system Hamiltonian ($\lambda_i = 0$) are plane waves:

$$|k\rangle = \frac{1}{\sqrt{N}}\sum_{x=1}^{L}\sum_{y=1}^{L}\exp\left(ik_x x + ik_y y\right)\hat{c}_x^\dagger\hat{c}_y^\dagger|0\rangle, \tag{14}$$

where $k_x$ and $k_y$ are the wave vectors lying in the first Brillouin zone, i.e., $k_x \in (-\pi/a \quad, \pi/a]$ and $k_y \in (-\pi/a \quad, \pi/a]$ with lattice spacing $a$ and $N = L \times L$ (square lattice). The corresponding eigenvalue of the system Hamiltonian is $E = 2t[\cos(k_x a) + \cos(k_y a)]$. After performing sudden quench of $\lambda_i = 0$ to $\lambda_f = \infty$, the Loschmidt amplitude can be written as

$$G(\lambda_f, \tau) = \langle k|e^{-i\tau\tilde{H}(\lambda_f)}|k\rangle, \tag{15}$$

$$= \sum_{x=1}^{L}\sum_{y=1}^{L}\langle k|e^{-i\tau\hat{H}(\lambda_f)}|\Psi_{xy}(\lambda_f)\rangle\langle\Psi_{xy}(\lambda_f)|k\rangle,$$

$$= \sum_{x=1}^{L}\sum_{y=1}^{L}e^{-i\tau E_{xy}}|\langle\Psi_{xy}(\lambda_f)|k\rangle|^2, \tag{16}$$

where $E_{xy}$ and $\Psi_{xy}(\lambda_f)$ denote the eigenspectrum and eigenstate of the postquench system Hamiltonian, respectively. In the limit, $\lambda_f \to \infty$, the eigenstates of the system Hamiltonian are localized on a single site, $|\Psi_{xy}\rangle$,

$$|\Psi_{xy}(\varepsilon_{x,y} = \infty)\rangle = \sum_{i=1}^{L}\sum_{j=1}^{L}\delta_{ix}\delta_{jy}\hat{c}_i^\dagger\hat{c}_j^\dagger|0\rangle. \tag{17}$$

Plugging (17) into (16), we obtain

$$G(\lambda_f, \tau) = \frac{1}{N}\sum_{x=1}^{L}\sum_{y=1}^{L}e^{-i\tau\lambda_f[\cos(2\pi\gamma x)+\cos(2\pi\gamma y)]}. \tag{18}$$

The phases $\theta = 2\pi\gamma x$ and $\phi = 2\pi\gamma y$ for an irrational number $\alpha$ are randomly distributed between $-\pi$ and $\pi$ in the thermodynamic limit. Therefore, we may approximate the expression (18) by replacing summation over integration, which reads

$$G(\lambda_f, \tau) = \frac{1}{(2\pi)^2}\int_{-\pi}^{\pi}\int_{-\pi}^{\pi}d\theta\, d\phi e^{-i\tau\lambda_f[\cos(\theta)+\cos(\phi)]},$$

$$= J_0^2(\lambda_f\tau). \tag{19}$$

The Loschmidt echo turns out to be

$$L(\lambda_f, \tau) = \left|J_0^2(\lambda_f\tau)\right|^2, \tag{20}$$

where $J_0(x_s)$ is the zero-order Bessel function of the first kind and has a series of zeros at critical times $\tau_s^* = x_s/\lambda_f$, with $s$ the set of positive roots. In the small $s$ limit, the roots of $J_0(x_s)$ can be computed approximately by Stokes' s approximation:

$$x_s = \frac{\mu}{4}\left(1 + \frac{2}{\mu^2} - \frac{62}{3\mu^4} + \frac{7558}{15\mu^6}\right), \quad \mu = \pi(4s - 1). \tag{21}$$

The most peculiar property of the quantum quenched system is the occurrence of a series of zeros of the Loschmidt echo at critical times, known as the DQPTs. An absolute error of the Loschmidt echo $|\Delta L(\tau)| = |L(\tau) - \tilde{L}(\tau)|$ for the 2D AA model is illustrated in Fig. 4. Here, $L(\tau)$ and $\tilde{L}(\tau)$

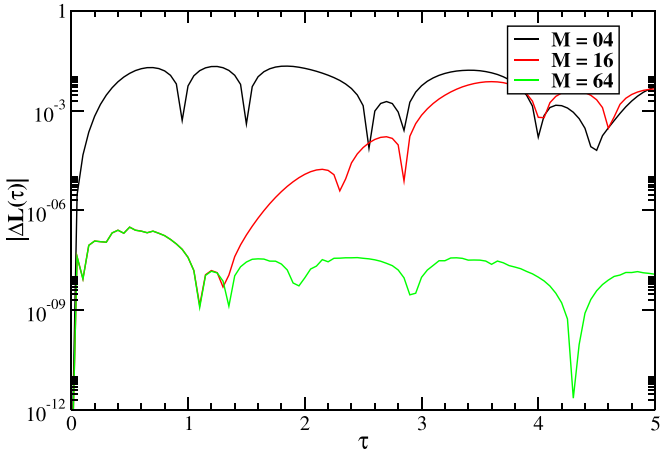


FIG. 4. Absolute error of the Loschmidt echo, $|\Delta L(\tau)|$, for an initially localized state quenched into a time-dependent state with $\lambda_f = 0.3$ in log-linear scale. Numerical calculations are carried out for a system of linear size $L = 100$ using exact diagonalization and KPM with different degree of expansion coefficients.

represent Loschmidt echos computed by using an exact diagonalization method (EDM) and KPM, respectively. Numerical calculations are carried out for an initially localized state of the system of size $L = 100$ with $\lambda_f = 0.3$. Remarkably, for sufficiently large Chebyshev moments, the KPM procedure computes accurate numerical results in the quench dynamics.

Now we turn to the case where an initially ground state of the prequench Hamiltonian with an infinite diagonal potential ($\lambda_i \to \infty$) is quenched into an extended time-evolved state of the postquench Hamiltonian with zero diagonal potential. In this limit, $\lambda_i \to \infty$, the initial eigenstates of the system Hamiltonian are localized at a single site, $|\Psi_{xy}\rangle$. The Loschmidt amplitude in this case can be written as

$$\begin{aligned} G(\tau) &= \langle\Psi_{xy}|e^{-i\tau\tilde{H}(\lambda_f)}|\Psi_{xy}\rangle, \qquad (22)\\ &= \sum_{k_x}\sum_{k_y}\langle\Psi_{xy}|e^{-i\tau\hat{H}(\lambda_f)}|k\rangle\langle k|\Psi_{xy}\rangle,\\ &= \sum_{k_x}\sum_{k_y} e^{-i\tau E}|\langle\Psi_{xy}|k\rangle|^2,\\ &= \frac{1}{N}\sum_{k_x}\sum_{k_y} e^{-2i\tau[\cos(k_x a)+\cos(k_y a)]}. \qquad (23)\end{aligned}$$

In the large-$N$ limit, we can replace the summation by the integration, which reads

$$\begin{aligned} G(\lambda_f,\tau) &= \frac{a^2}{(2\pi)^2}\int_{-\frac{\pi}{a}}^{\frac{\pi}{a}}\int_{-\frac{\pi}{a}}^{\frac{\pi}{a}} dk_x\, dk_y e^{-2i\tau\left(\cos k_x a+\cos k_y a\right)},\\ &= J_0^2(2\tau). \qquad (24)\end{aligned}$$

The Loschmidt echo has the form

$$L(\tau) = \left|J_0^2(2\tau)\right|^2. \qquad (25)$$

From this expression, it is clear that the Loschmidt echo is nonanalytic at critical times $\tau^* = x_s/2$, reflecting the DQPTs in the system. Moreover, this transition turns out to be $\lambda_f$ independent in the thermodynamic limit. An EDM is used to numerically calculate the Loschmidt echo of the system, which turns out to be computationally costly and limited to small system sizes. In order to overcome this problem, we employ the KPM [53], which allows us to compute the Loschmidt echo efficiently for infinitely large systems without exactly diagonalizing the system Hamiltonian. The KPM is a polynomial expansion-based method that computes various physical quantities with controlled accuracy at a moderate computational cost. It makes use of Chebyshev polynomial expansion, which has good convergence properties [79], together with optimal damping kernels. However, it turns out that accuracy and numerical convergence can be controlled only by using large enough polynomial moments without optimal damping kernels, reflecting the continuously differentiable nature of the Loschmidt echo.

Note that for the KPM implementations, the Hamiltonian spectrum and all the associated energy scales must be normalized in the standard range of orthogonality of the Chebyshev polynomials ($[-1\ 1]$). Thus, dividing the Hamiltonian and all energy scales by a positive energy scale $(4 + 2\lambda)$ will impose the normalization condition. Next, we define the set of Chebyshev polynomials:

$$T_m(z) = \cos[m\ \arccos(z)], \quad m \in \mathbb{N}, \qquad (26)$$

where $T_m(z)$ denotes the $m$th degree Chebyshev polynomials of the first kind. Moreover, the $T_m(z)$'s obey the following recurrence relation:

$$T_m(z) = 2zT_{m-1}(z) - T_{m-2}(z), \quad m > 1, \qquad (27)$$

starting with $T_0(z) = 1$ and $T_1(z) = z$, and also satisfying the orthogonality relation,

$$\begin{aligned}\langle T_n(z)|T_m(z)\rangle &= \frac{1}{\pi}\int_{-1}^{1} T_n(z)T_m(z)(1-z^2)^{-1/2}\,dz,\\ &= \frac{1}{2}\delta_{n,m}(\delta_{n,0}+1).\end{aligned}$$

For the KPM estimates of Loschmidt amplitude, we make use of the identity [80],

$$e^{-iz\tau} = \sum_{m=0}^{\infty}\frac{2i^{-m}}{1+\delta_{m,0}}J_m(\tau)T_m(z), \quad |z| \leqslant 1, \qquad (28)$$

for the $e^{-iH\tau}$ part of Loschmidt amplitude. Here $J_m(z)$ is the Bessel function of $m$th order. The expansion of $e^{-iH\tau}$ in terms of the Chebyshev polynomial becomes

$$e^{-i\tilde{H}\Omega\tau} = \sum_{m=0}^{\infty}\frac{2i^{-m}}{1+\delta_{m,0}}J_m(\Omega\tau)T_m(\tilde{H}), \qquad (29)$$

where $\tilde{H} = H/\Omega$ is the rescaled Hamiltonian of the system and $\Omega$ is a positive energy scale that normalizes the Hamiltonian to place its spectrum within $[-1\ ,\ 1]$. The KPM estimates of Loschmidt amplitude, $\tilde{G}(\alpha,\beta,\tau)$, have the following form:

$$\tilde{G}(\alpha,\beta,\tau) = \sum_{m=0}^{\infty}\frac{2i^{-m}}{1+\delta_{m,0}}J_m(\Omega\tau)\langle\Psi(\alpha)|T_m[\tilde{H}(\beta)]|\Psi(\alpha)\rangle. \qquad (30)$$

Note that the KPM expansion in practical numerical calculations can be carried out only for a finite Chebyshev series.

Hence, the truncated form of the Loschmidt amplitude is

$$\tilde{G}(\alpha,\beta,\tau)=\sum_{m=0}^{M-1}\frac{2i^{-m}}{1+\delta_{m,0}}J_m(\Omega\tau)\langle T_m[\tilde{H}(\beta)]\rangle, \tag{31}$$

where

$$\langle T_m(\tilde{H}(\beta))\rangle=\langle\Psi(\alpha)|T_m[\tilde{H}(\beta)]|\Psi(\alpha)\rangle \tag{32}$$

is the expectation value of the Chebyshev polynomials in the Hamiltonian (31) shows the truncated KPM approximations of the Loschmidt amplitude. It is worthwhile to mention that the truncated expansions for nondifferentiable functions lead to unwanted oscillations known as Gibbs oscillations which can be eliminated by using an optimized damping factor [53]. However, a Loschmidt echo is a differentiable function whose accuracy and numerical convergence can be controlled only by using large enough Chebyshev moments.

The main focus is to employ the KPM algorithm for the numerical calculations of the Loschmidt echo when an initial eigenstate [$|\Psi(\alpha)\rangle$] is either extended or localized. In the absence of on-site potential, the eigenstates of the system Hamiltonian are plane waves, $|\Psi(\alpha)\rangle=|k\rangle$. On the other hand, in the presence of an infinite diagonal potential ($\varepsilon_{x,y}\to\infty$), the initial eigenstates of the system Hamiltonian are localized on a single site $ij$.

The expectation value of Chebyshev polynomials in the Hamiltonian can be handled straightforwardly by using the recursion relations for the $T_m(z)$ [Eq. (27)]. Starting from the initial state $|\Psi(\alpha)\rangle$, we can iteratively construct the expectation value of $T_m[\tilde{H}(\beta)]$ as

$$\langle T_0[\tilde{H}(\beta)]\rangle=\langle\Psi(\alpha)|T_0[\tilde{H}(\beta)]|\Psi(\alpha)\rangle=1, \tag{33}$$

$$\langle T_1[\tilde{H}(\beta)]\rangle=\langle\Psi(\alpha)|\tilde{H}(\beta)|\Psi(\alpha)\rangle=\langle\tilde{H}(\beta)\rangle, \tag{34}$$

and for $m>1$,

$$\langle T_m[\tilde{H}(\beta)]\rangle=2\langle\tilde{H}(\beta)\rangle\langle T_{m-1}[\tilde{H}(\beta)]\rangle-\langle T_{m-2}[\tilde{H}(\beta)]\rangle. \tag{35}$$

It is noted that the numerical complexity of the KPM algorithm for the calculations of Loschmidt echo scales as $O(MN)$ for a sparse matrix of the system Hamiltonian, where $N$ is the system size and $M$ is the number of Chebyshev moments. The time-consuming part of the algorithm is the iterative computation of the expectation value $\langle T_m[\tilde{H}(\beta)]\rangle$, costing $O(N)$ numerical complexity. The $O(M)$ comes from the summing over the Chebyshev series. However, the computational cost becomes $O(MN^2)$ for a dense Hamiltonian matrix due to multiplications for all elements of $\tilde{H}(\beta)$ and the initial state $|\Psi(\alpha)\rangle$. As stated above, the numerical convergence and resolutions of the KPM estimates of the Loschmidt echo are controlled by the number of Chebyshev series ($M$). This means that the absolute difference between the exact $L(\alpha,\beta,\tau)$ and KPM estimates of the Loschmidt echo $\tilde{L}(\alpha,\beta,\tau)$ goes to zero,

$$|L(\alpha,\beta,\tau)-\tilde{L}(\alpha,\beta,\tau)|\to 0, \tag{36}$$

for sufficiently large Chebyshev series in the $N\to\infty$ limit. The KPM estimates converge uniformly for a sufficiently large Chebyshev series.

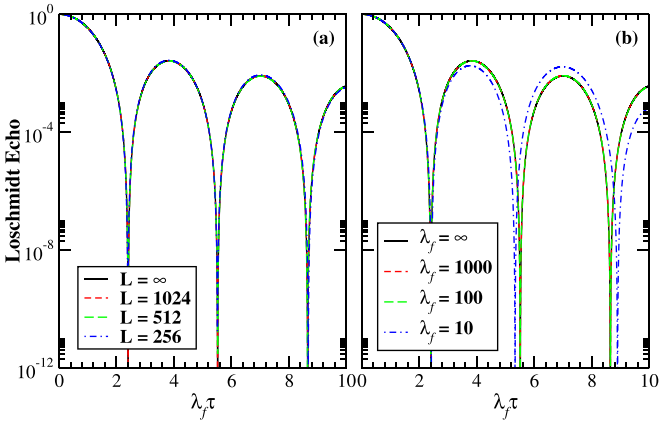


FIG. 5. The quench dynamics of the 2D Aubry-André model, when an initial ground state (plane wave) is quenched into a time-evolved strongly localized regime ($\lambda_f\to\infty$). The evolution of the Loschmidt echo for various (a) linear system sizes and (b) postquench modulation potential amplitudes. All computations are carried out for a system with periodic boundary conditions (PBCs) with $M=1024$ Chebyshev moments and a wave vector $k_x=k_y=\pi/2$. The black bold curve corresponds to the analytical result [Eq. (20)] obtained in the thermodynamic limit. A logarithmic scale has been chosen to highlight the zeros of the Loschmidt echo.

Our goal is to efficiently compute the KPM estimates of the Loschmidt echo under the quantum quenched 2D Aubry-André model, where the quench dynamics are induced by a sudden change in the diagonal potential strength. First, we consider a limiting case when an initial ground state (plane wave) is quenched into a strongly localized time-evolved state ($\lambda_f\to\infty$). In order to validate the KPM algorithm, we compute the numerical approximation of the Loschmidt echo in the large postquench modulation potential strength, as illustrated in Fig. 5(a). Here the KPM simulations are carried out for various linear system sizes with PBC, $M=1024$ Chebyshev moments, $\lambda_i=0$, $\lambda_f=1000$, and wave vector $k_x=k_y=\pi/2$. Elegantly, we find an excellent agreement between the KPM estimates of the Loschmidt echo and the analytical result (black bold curve) in the strong potential limit, confirming the validity of the KPM procedure. Most importantly, the Loschmidt echo turns out to be zero periodically at critical times, reflecting the DQPTs in the system. We also study the role of postquench modulation potential on the time evolutions of the Loschmidt echo, as shown in Fig. 5(b). It is noted that the zeros of the Loschmidt echo deviate from the analytical result in the weak postquench modulation potential limit ($\lambda_f=10$), but start to converge with increasing potential. This shows that the system exhibits DQPTs as long as the time-evolved state is in the localized regime ($\lambda_f>2$).

We now discuss the nonequilibrium dynamics under the prequench localized and postquench extended states of the model. We observe excellent agreement of the numerical data with the analytical result obtained in the thermodynamic limit (black bold curve), confirming the KPM method as depicted in Fig. 6(a). The numerical calculations are performed for various system sizes, $M=1024$ Chebyshev moments, $\lambda_i=1000$, and $\lambda_f=0$. Analogous to the previous case, the system exhibits DQPTs, characterized by the nonanalytic behavior of

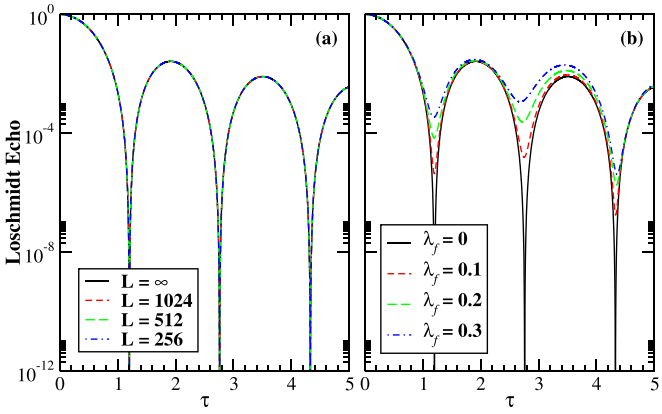


FIG. 6. The quench dynamics of the 2D Aubry-André model, when an initially localized state ($\lambda_i \to \infty$) is quenched into a time-evolved extended regime ($\lambda_f = 0$). The evolution of the Loschmidt echo for various (a) linear system sizes and (b) postquench modulation potential amplitudes. All computations are carried out for a system with PBCs and $M = 1024$ Chebyshev moments. The black bold curve corresponds to the analytical result [Eq. (25)] obtained in the thermodynamic limit. A logarithmic scale has been chosen to highlight the zeros of the Loschmidt echo.

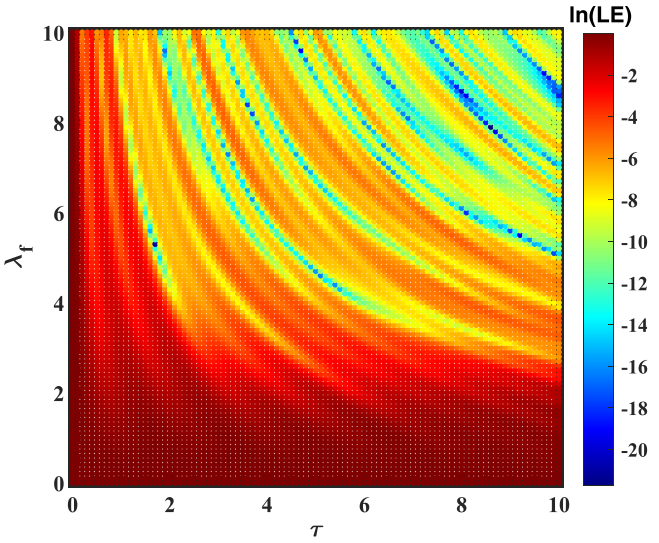


FIG. 7. Time evolution of the logarithm of the Loschmidt echo as a function of postquench potential $\lambda_f$ and evolving time $\tau$. Numerical computations are performed for an initially localized state ($\lambda_i \to \infty$) quenched into a time-evolved state for a system of linear size $L = 1024$ with $M = 1024$ Chebyshev moments.

the Loschmidt echo at critical times. However, for a fixed system size, the singularities are progressively broadened (smoothed out) with increasing postquench potential strength, as shown in Fig. 6(b). This means that the system will display no DQPTs in the limit of strong potential strength ($\lambda_f > 2$). In fact, in this limit, both the initial and its time-evolved states are in the localized regime. As a consequence, the overlap between the two localized states yields a finite value.

To get a better understanding of the quench dynamics around the critical point $\lambda_f = 2$, we numerically calculate the KPM estimates of the logarithm of the Loschmidt echo in the time–potential plane for an initial localized state that is quenched into a time-evolved state of the Hamiltonian with incommensurate potential. At $\tau = 0$, one can obviously get the maximum Loschmidt echo [$\ln(LE) = 0$], resulting from the overlap of the two plane waves as presented in Fig. 7. However, after a certain time interval, the Loschmidt echo for $\lambda_f < 2$ turns out to decay to zero periodically, predicting DQPTs in the quenched system. On the other hand, the system displays no DQPTs for an extended time-evolved state of the system Hamiltonian ($\lambda_f > 2$). The logarithm of the Loschmidt echo in this case remains finite and negative at any instant of time. Remarkably, the negative value of the logarithm of the Loschmidt echo predicts the nonexistence of the DQPTs.

## IV. NUMERICAL COMPLEXITY

The numerical complexity of the polynomial expansion method for tailoring the nonequilibrium dynamics is $O(MN)$ for a sparse and $O(MN^2)$ for a dense matrix of the system Hamiltonian, where $O(N)$ is the system size of the square lattice and $M$ is the number of Chebyshev series. Here we perform a set of KPM simulations for the system with different system sizes in order to estimate the computational time (sec) and memory usage (GB). The numerical calculations are carried out for quench dynamics, where an initial plane wave is quenched into a time-evolved state of the system Hamiltonian with $\lambda_f = 10$ (localized time-evolved state). It is important to mention that the numerical data converge to analytical data for sufficiently large system sizes with $M = 1024$ Chebyshev moments. Thus, by keeping the moments fixed, we estimate the computational time and memory usage for

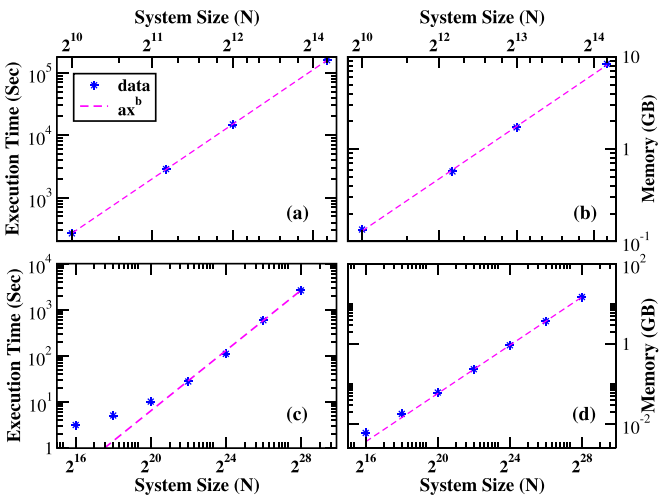


FIG. 8. Scaling of the (a), (c) execution time (sec) and (b), (d) memory usage (GB) for calculating the Loschmidt echo of the model based on the EDM (upper panels) and the polynomial-expansion technique (lower panels) in log-log scale. Numerical computations are performed for an initial plane wave ($k = \pi/2$) quenched to a time-evolved state with $\lambda_f = 10$ for the 2D model with $M = 1024$ Chebyshev moments. Numerical data are very well fitted to $ax^b$ (magenta dashed lines), (a) $b = 2.9$, and (c) $b = 1.085$ for the execution time, and (b) $b = 1.88$ and (d) $b = 0.999$ for the memory usage.

the simulation. For the sparse matrix Hamiltonian, the size scaling of the execution time and memory usage are illustrated in Fig. 8. Importantly, the execution time and memory usage are very well fitted to $ax^b$ for large system sizes, where $a$ and $b$ are real constants. It is clearly shown that the execution time and memory usage of the EDM are approximately scaled as $N^{2.9}$ and $N^{1.8}$ for a sparse Hamiltonian matrix obtained by fitting the data as shown by the magenta dashed line in Figs. 8(a) and 8(b), respectively. Most importantly, the KPM algorithm proves to be an efficient numerical method with a computational cost as well as memory usage scale linearly with the system size, as illustrated in Figs. 8(c) and 8(d), respectively. This shows that the higher numerical complexity of the EDM technique can be successfully circumvented by using the polynomial-expansion scheme.

## V. CONCLUSION

We have investigated the localization properties of the noninteracting tight-binding 2D Aubry-André model. We have pointed out that the IPR starts to increase, whereas the NPR drops to zero at $\lambda = 2$, signaling a metal-insulator transition in the system. Moreover, we have shown that the model exhibits self-duality at critical diagonal incommensurate potential, leading to an energy-independent Anderson transition. Moreover, we pointed out that the fidelity susceptibility has divergent behavior around $\lambda = 2$, verifying the metal-insulator transition. Furthermore, we investigated the nonequilibrium dynamics of the noninteracting tight-binding 2D Aubry-André model by quenching the disorder strength. We have performed numerical simulations of quench dynamics in the model using an efficient numerical technique based on the polynomial expansion method. We observed that the quench dynamics trigger the DQPTs, characterized by the nonanalyticities in the Loschmidt echos at critical times. The numerical results agree with the analytical calculations obtained for the infinite on-site potential in the thermodynamic limit. In addition, the computational cost of the Loschmidt echo simulations is greatly reduced by applying the polynomial expansion approach, which scales linearly with the system size.

## ACKNOWLEDGMENTS

N.A.K. gratefully acknowledges the postdoctoral fellowship supported by Zhejiang Normal University under Grant No. ZC304022980. G.X. acknowledges support from the NSFC under Grants No. 11835011 and No. 12174346.

[1] S. Aubry and G. André, Ann. Israel Phys. Soc. **3**, 133 (1980).
[2] Z. M. Stadnik, *Physical Properties of Quasicrystals* (Springer, Berlin, 2012).
[3] J. B. Sokoloff, Phys. Rev. B **23**, 6422 (1981).
[4] S. Das Sarma, S. He, and X. C. Xie, Phys. Rev. Lett. **61**, 2144 (1988).
[5] J. Biddle and S. Das Sarma, Phys. Rev. Lett. **104**, 070601 (2010).
[6] Y. E. Kraus, Y. Lahini, Z. Ringel, M. Verbin, and O. Zilberberg, Phys. Rev. Lett. **109**, 106402 (2012).
[7] X. Cai and Y.-C. Yu, J. Phys.: Condens. Matter **35**, 035602 (2022).
[8] T. Liu and X. Xia, Phys. Rev. B **105**, 054201 (2022).
[9] T. Liu and S. Cheng, Chin. Phys. B **32**, 027102 (2023).
[10] S. Longhi, Phys. Rev. B **107**, 134203 (2023).
[11] M. Johansson and R. Riklund, Phys. Rev. B **43**, 13468 (1991).
[12] M. Yahyavi, B. Hetényi, and B. Tanatar, Phys. Rev. B **100**, 064202 (2019).
[13] F. A. An, K. Padavić, E. J. Meier, S. Hegde, S. Ganeshan, J. H. Pixley, S. Vishveshwara, and B. Gadway, Phys. Rev. Lett. **126**, 040603 (2021).
[14] C. Aulbach, A. Wobst, G. L. Ingold, P. Hänggi, and I. Varga, New J. Phys. **6**, 70 (2004).
[15] F. A. An, E. J. Meier, and B. Gadway, Phys. Rev. X **8**, 031045 (2018).
[16] H. P. Lüschen, S. Scherg, T. Kohlert, M. Schreiber, P. Bordia, X. Li, S. Das Sarma, and I. Bloch, Phys. Rev. Lett. **120**, 160404 (2018).
[17] Y. Lahini, R. Pugatch, F. Pozzi, M. Sorel, R. Morandotti, N. Davidson, and Y. Silberberg, Phys. Rev. Lett. **103**, 013901 (2009).
[18] V. Goblot, A. Štrkalj, N. Pernet, J. L. Lado, C. Dorow, A. Lemaître, L. Le Gratiet, A. Harouri, I. Sagnes, S. Ravets *et al.*, Nat. Phys. **16**, 832 (2020).
[19] H. Li, Y.-Y. Wang, Y.-H. Shi, K. Huang, X. Song, G.-H. Liang, Z.-Y. Mei, B. Zhou, H. Zhang, J.-C. Zhang *et al.*, npj Quantum Inf. **9**, 40 (2023).
[20] N. Mott, J. Phys. C: Solid State Phys. **20**, 3075 (1987).
[21] S. Ganeshan, J. H. Pixley, and S. Das Sarma, Phys. Rev. Lett. **114**, 146601 (2015).
[22] Y. Wang, J.-H. Zhang, Y. Li, J. Wu, W. Liu, F. Mei, Y. Hu, L. Xiao, J. Ma, C. Chin, and S. Jia, Phys. Rev. Lett. **129**, 103401 (2022).
[23] T. Liu, H. Guo, Y. Pu, and S. Longhi, Phys. Rev. B **102**, 024205 (2020).
[24] T. Liu, S. Cheng, H. Guo, and G. Xianlong, Phys. Rev. B **103**, 104203 (2021).
[25] W. Chen, S. Cheng, J. Lin, R. Asgari, and G. Xianlong, Phys. Rev. B **106**, 144208 (2022).
[26] D. Peng, S. Cheng, and G. Xianlong, Phys. Rev. B **107**, 174205 (2023).
[27] Z.-H. Xu, X. Xia, and S. Chen, Sci. China-Phys. Mech. Astron. **65**, 227211 (2022).
[28] C. Chiaracane, M. T. Mitchison, A. Purkayastha, G. Haack, and J. Goold, Phys. Rev. Res. **2**, 013093 (2020).
[29] M. Heyl, Phys. Rev. Lett. **115**, 140602 (2015).
[30] M. Heyl, F. Pollmann, and B. Dóra, Phys. Rev. Lett. **121**, 016801 (2018).
[31] M. Heyl, Rep. Prog. Phys. **81**, 054001 (2018).
[32] C. Yang, Y. Wang, P. Wang, X. Gao, and S. Chen, Phys. Rev. B **95**, 184201 (2017).
[33] H. Yin, S. Chen, X. Gao, and P. Wang, Phys. Rev. A **97**, 033624 (2018).

[34] K. Xu, Z.-H. Sun, W. Liu, Y.-R. Zhang, H. Li, H. Dong, W. Ren, P. Zhang, F. Nori, D. Zheng *et al.*, Sci. Adv. **6**, eaba4935 (2020).
[35] X. Tong, Y.-M. Meng, X. Jiang, C. Lee, Gentil Dias de Moraes Neto, and G. Xianlong, Phys. Rev. B **103**, 104202 (2021).
[36] F. Zhou, J. Williams, S. Sun, C. D. Malliakas, M. G. Kanatzidis, A. F. Kemper, and C.-Y. Ruan, Nat. Commun. **12**, 566 (2021).
[37] M. Van Damme, T. V. Zache, D. Banerjee, P. Hauke, and J. C. Halimeh, Phys. Rev. B **106**, 245110 (2022).
[38] L.-J. Zhai, G.-Y. Huang, and S. Yin, Phys. Rev. B **106**, 014204 (2022).
[39] C. Y. Wong and W. C. Yu, Phys. Rev. B **105**, 174307 (2022).
[40] S. Gaur, V. Gurarie, and E. A. Yuzbashyan, Phys. Rev. B **106**, L220506 (2022).
[41] N. A. Khan, X. Wei, S. Cheng, M. Jan, and G. Xianlong, Phys. Lett. A **475**, 128880 (2023).
[42] N. A. Khan, P. Wang, M. Jan, and G. Xianlong, Sci. Rep. **13**, 9470 (2023).
[43] Y.-T. Zou and C. Ding, Phys. Rev. B **108**, 014303 (2023).
[44] S. Ye, Z. Zhou, N. A. Khan, and G. Xianlong, Phys. Rev. A **109**, 043319 (2024).
[45] N. A. Khan, Chaos, Solitons Fractals **183**, 114975 (2024).
[46] D. Chen, M. White, C. Borries, and B. DeMarco, Phys. Rev. Lett. **106**, 235304 (2011).
[47] M. Schmitt, M. M. Rams, J. Dziarmaga, M. Heyl, and W. H. Zurek, Sci. Adv. **8**, eabl6850 (2022).
[48] X. Nie, B.-B. Wei, X. Chen, Z. Zhang, X. Zhao, C. Qiu, Y. Tian, Y. Ji, T. Xin, D. Lu, and J. Li, Phys. Rev. Lett. **124**, 250601 (2020).
[49] J. H. Wilkinson, *The Algebraic Eigenvalue Problem* (Oxford University Press, New York, 1988).
[50] A. Bjelčić, T. Nikšić, and Z. Drmač, Comput. Phys. Commun. **280**, 108477 (2022).
[51] Z. Fan, J. H. Garcia, A. W. Cummings, J. E. Barrios-Vargas, M. Panhans, A. Harju, F. Ortmann, and S. Roche, Phys. Rep. **903**, 1 (2021).
[52] Y. Li, Z. Zhan, X. Kuang, Y. Li, and S. Yuan, Comput. Phys. Commun. **285**, 108632 (2023).
[53] A. Weiße, G. Wellein, A. Alvermann, and H. Fehske, Rev. Mod. Phys. **78**, 275 (2006).
[54] S. M. João, M. Andelkovic, L. Covaci, T. G. Rappoport, J. M. V. P. Lopes, and A. Ferreira, R. Soc. Open Sci. **7**, 191809 (2020).
[55] S. M. João, J. M. V. P. Lopes, and A. Ferreira, J. Phys. Mater. **5**, 045002 (2022).
[56] N. A. Khan, J. M. V. P. Lopes, J. P. S. Pires, and J. M. B. L. dos Santos, J. Phys.: Condens. Matter **31**, 175501 (2019).
[57] L.-W. Wang, Phys. Rev. B **49**, 10154 (1994).
[58] G. Chen, F. Song, and J. L. Lado, Phys. Rev. Lett. **130**, 100401 (2023).
[59] N. A. Khan, Chin. J. Phys. **85**, 733 (2023).
[60] L. Covaci, F. M. Peeters, and M. Berciu, Phys. Rev. Lett. **105**, 167006 (2010).
[61] N. A. Khan and S. T. Amin, Phys. Scr. **96**, 045812 (2021).
[62] S. G. de Castro, A. Ferreira, and D. A. Bahamon, Phys. Rev. B **107**, 045418 (2023).
[63] N. A. Khan, W. Chen, M. Jan, and G. Xianlong, Comput. Phys. Commun. **299**, 109132 (2024).
[64] M. Rossignolo and L. Dell'Anna, Phys. Rev. B **99**, 054211 (2019).
[65] A. Szabó and U. Schneider, Phys. Rev. B **101**, 014205 (2020).
[66] A. Štrkalj, E. V. H. Doggen, and C. Castelnovo, Phys. Rev. B **106**, 184209 (2022).
[67] P. Zanardi and N. Paunković, Phys. Rev. E **74**, 031123 (2006).
[68] W.-L. You, Y.-W. Li, and S.-J. Gu, Phys. Rev. E **76**, 022101 (2007).
[69] A. F. Albuquerque, F. Alet, C. Sire, and S. Capponi, Phys. Rev. B **81**, 064418 (2010).
[70] L. Wang, Y.-H. Liu, J. Imriška, P. N. Ma, and M. Troyer, Phys. Rev. X **5**, 031007 (2015).
[71] Q. Luo, J. Zhao, and X. Wang, Phys. Rev. E **98**, 022106 (2018).
[72] Z. Zhu, G. Sun, W.-L. You, and D.-N. Shi, Phys. Rev. A **98**, 023607 (2018).
[73] B.-B. Wei and X.-C. Lv, Phys. Rev. A **97**, 013845 (2018).
[74] B.-B. Wei, Phys. Rev. A **99**, 042117 (2019).
[75] G. Sun, B.-B. Wei, and S.-P. Kou, Phys. Rev. B **100**, 064427 (2019).
[76] X.-J. Yu, S. Yang, J.-B. Xu, and L. Xu, Phys. Rev. B **106**, 165124 (2022).
[77] M. M. Oliveira, P. Ribeiro, and S. Kirchner, npj Quantum Inf. **9**, 6 (2023).
[78] S. De Nicola, A. A. Michailidis, and M. Serbyn, Phys. Rev. B **105**, 165149 (2022).
[79] J. Mason and D. Handscomb, *Chebyshev Polynomials* (CRC Press, New York, 2002).
[80] F. Iacopi, J. Boeckl, and C. Jagadish, *2D Materials* (Academic Press/Elsevier, New York, 2016).